SPECIAL ISSUE SHORT COMMUNICATION

INTERNATIONAL JOURNAL OF
ENERGY RESEARCH WILEY

Tropical fruit waste-derived mesoporous rock-like Fe₂O₃/C composite fabricated with amphiphilic surfactant-templating approach showing massive potential for high-tech applications

Paskalis Sahaya Murphin Kumar[1] | Sivarasan Ganesan[2] |
Ala'a H. Al-Muhtaseb[3] | Lamya Al-Haj[4] | Mari Elancheziyan[2] |
Sutha Shobana[5] | Gopalakrishnan Kumar[1,6]

[1]School of Civil and Environmental Engineering, Yonsei University, Seoul, South Korea

[2]Research Centre for Environmental medicine, Kaohsiung Medical University, Koahsiung, Taiwan

[3]Department of Petroleum and Chemical Engineering, College of Engineering, Sultan Qaboos University, Muscat, Oman

[4]Department of Biology, College of Science, Sultan Qaboos University, Muscat, Oman

[5]Department of Chemistry and Research Centre, Mohamed Sathak Engineering College, Ramanathapuram, India

[6]Institute of Chemistry, Bioscience and Environmental Engineering, Faculty of Science and Technology, University of Stavanger, Stavanger, Norway

Correspondence
Lamya Al-Haj, Department of Biology, College of Science, Sultan Qaboos University, Muscat, Oman.
Email: gopalakrishnanchml@yonsei.ac.kr; gopalakrishnan.kumar@uis.no

Gopalakrishnan Kumar, School of Civil and Environmental Engineering, Yonsei University, Seoul 03722, South Korea.
Email: gopalakrishnanchml@gmail.com

Summary

Recently, the glycolipids biosurfactant materials have widely been utilized for many industrial applications due to their feasible surface activity, biodegradable as well as eco-friendly nature. Even though many of the earlier studies have been reported on such kind of surfactants, in this study we focused on porous rocks-like Fe₂O₃/C composites, which were magnificently synthesized from a novel tropical fruit biomass, using a glycolipid biosurfactant with high specific surface area of about 466.9 m²/g via a biofunctional single-step thermo-chemical method. They could be applied as an adsorbent to adsorb the pharmaceutical pollutants mainly, DCF from aqueous solution. Moreover, the highest adsorption capacity for DCF could be achieved, which is of about 77.51 mg/g. Furthermore, as-prepared glycolipid functionalized Fe₂O₃/C composites were used as electrode materials for high-performance supercapacitors. Galvanostatic charge-discharge results showed that the Fe₂O₃/C modified electrode possesses a specific capacitance of about 374 F/g with a current density of 0.2 A/g and it has retained 84% of capacitance, even after 3000 cycles. The

remarkable performances are mainly due to the surface amendments of the Fe_2O_3/C composite, using biologically produced glycolipid surfactant, would have more favorable foreground towards the upcoming energy crises.

1 | INTRODUCTION

These days, issues on the fossil fuel energy demand and environmental contaminations have become more prominent. The AC materials present a 2D-macromolecule, containing amazing interfacial properties.[1,2] Due to huge surface area, and massive electrical conductivity, high mechanical power, and less density, ACs has been commonly employed newly for our environmental and energetical applications. The surface modified ACs present an improvement to the inherent properties of the raw carbon (RC), in the way of a high accessible rate, more flexibility and very strong mechanical strength owing to their highly porous interlinking structure.[3-5] Hence, porous activated carbon is broadly focused on both the adsorption and supercapacitance fields. Presently, many biowastes, along with rice husk,[6] paddy straw,[7] residual microalgae,[8] walnut shell, and rapeseed shell,[9] have been applied as starting sources to synthesis high surface carbon resources. All these materials possess deficient adsorbent and extraordinary potentiality as electrode provisions for energy storage applications. Hence, some of the demerits on biochar are its less active surface and inadequate porous nature,[10-12] which all restrict potential exploitation in environmental application, except its supplementary sustainable activation.[13-15] So far this challenging controversy may ultimately inhibit the synthesis methods. The organic or surfactant-templating route has been applied effectively to the fabrication of homogenous mesoporous materials for both organic and inorganic substrates.[16-18] Polymeric and amphiphilic biosurfactants can be accessed as a template to homogeneous mesoporous objects, with high surface areas and linear pore distributions that are performed for high-tech industrial applications.[19,20]

Furthermore, biosurfactant is a chemical component that is used in adhesives, emulsifiers, flocculators, wetting, and forming solutions, lubricants, and penetrants.[21,22] Now-a-days, several biomasses and nanomaterials are developed by using biosurfactants, because of their zero toxicity to environment, cheapest/very low-cost nature and high biocompatibility properties. So, they are highly suitable templates, that is, they contain high oxygen species, which are easily decomposable in nature.[23-26] Biosurfactants have been utilized to improve the homogenous high-tech surface porosity of hydrophobic substrates to enhance the biocompatibility, through digestion/recovery process.[27,28] Many treatments have been practiced for the treatment of highly toxic and persistent nature of the pharmaceutical antibiotics contaminated wastewater, like as AOP, adsorption, coagulation, membrane separation, and ionic liquid treatments.[29-32] Above those methods, adsorption is focused as few of the conventional techniques for pharmaceutical remediation, due to its easiness, eco-friendly approach and economical applicability. Surface tuned activated carbon contains large surface areas, which are microporous as well as their rich pore shapes have been commercialized as adsorbents to industrial applications. Also, many naturally availed biomass-based adsorbents have been conveyed for treating pharmaceutical drugs like DCF, from wastewater. Lonappan et al[33] investigated two different biomasses, they were pinewood and pig manure into ACs and it is found that maximum adsorption rate was achieved in the range of 0.5 and 12.5 mg/g, respectively. Larous and Meniai[34] developed olive stones as a carbon precursor for the preparation of ACs and found that its maximum adsorption profit is 11 mg/g. Daniel et al[35] used cocoa pod husks as adsorbents to prepare potential ACs and get that its highest adsorption rate for DCF, achieved 5.4 mg/g. Coimbra et al[36] prepared ACs by pyrolysis of pulp mill sludge at 800°C and achieved that its DCF adsorption amount is 19.9 mg/g. Antunes et al[37] utilized Isabel grape bagasse as carbon sources to synthesis ACs and found that maximum DCF adsorption capacity is 76.9 mg/g. In addition, for the contribution to the water remedies, porous ACs have also found for application potentiality in the supercapacitance studies. Based on the merits of ultimate current density, long life cycling, noble electrical conductivity, eco-friendly, and feasibility, the supercapacitors are examined for their advanced energy storage plans.[38-40] They also possess chemical/thermal stability, quick charging/discharging feature, and high power density.[41] Moreover, the carbon-based electrode materials in making the supercapacitors for renewable and sustainable electrochemical energy storage systems mainly consist of carbon shells along with

interior voids with high encapsulation ability to increase the contact area between electrodes and electrolytes, ratios for surface to volume, good mechanical strength, low specific density, and tunable porosity.[41-43] The role of carbon shells not only facilitate the volume expansion/contraction, but also assist the electron transfer during charge storage process that eventually leads to cycling stability and outstanding performance of electrochemical energy storage systems.[41,44] The mechanism involved in such systems is significantly based on the facts that electrical doublelayer capacitance and pseudocapacitance, due to the electrostatic adsorption of ions on the surface and the fast and reversible Faradaic reactions at / near the surface of active materials, respectively. The reaction mechanism in the electrical doublelayer capacitance depends on the redox pathways that involve intercalation of ions of the active materials with N, O like heteroatoms and functional groups.[41,44] In the same way, the reaction mechanism in pseudocapacitance have aroused due to redox reactions of the doped heteroatoms.[41,45] The reaction to enhance the capacitance also depends on size match of the existing micropores in carbon for the electrolyte ions, the improvement of surface wettability, electrical conductivity, and electron-donor tendency of the carbon matrices.[41,46,47]

In this regard, herein we report a simple as well as feasible synthesis of homogenous mesoporous carbon framework of amphiphilic biosurfactant using templating approach, which was derived from tropical waste fruit biomass. *Crescentia cujete* (*Cc*) is a sustainable and sufficiently available tropical species and is a novel starting precursor for the synthesis of high-surface ACs. In this framework, we have chosen the *Cc* fruit shell as a precursor for the synthesis via plant-based biosurfactants (glycolipid) functionalized, magnetized rock-like Fe_2O_3/porous carbon composites as an adsorbent of DCF from the contaminated water and fabricated in supercapacitor electrodes. To be the end, the findings are shown and discussion is addressed in Figure 1. Further, the so produced *Crescentia cujete* biomass products of RC, glycolipid supported activated carbon (GAC), and glycolipid supported magnetic activated carbon (GMAC) are commonly mentioned as CCBs. The chemical activation between the biochar precursor and the glycolipid impregnated Fe_2O_3 provides some elasticity for the precursor materials due to the formation of inter lipid hydrogen bonding by the polar carbohydrate head with a linkage of 1,2-/1,3-di-O-acyl/alkyl-*sn*-glycerol in lipids, which leads to separation of the cellulosic fibres via partial depolymerization, followed by dehydration and condensation of the main cellular components viz. hemicellulose and lignin from the precursor matrix, thereby a decrease in mechanical resistance. This fact protects some additional cross-linking for the development of carbon porosity, which

may strongly be induced by the presence of glycolipid functionalized metal ionic species.[48]

2 | MATERIALS AND METHODS

All the experimental chemicals were purchased analytically by standard chemical companies. Deionized ultra-pure water is used for the preparation of all the experimental solutions.

2.1 | Synthesis of glycolipid

Pseudomonas mosselii (**F01**), bacteria were screened and production was achieved, using weed as a substrate. It is a milestone to *Parthenium hysterophorus* weed eradication and biosurfactants were produced, allowed for characterization and confirmed the presence of glycolipid biosurfactant functional groups.[49]

2.2 | Sampling and separation of microorganisms

Bacterial samples were collected from oil-exploration areas of diary as well as rice mills industrial effluents from Tiruvannamalai, Tamil Nadu in the South India.[50,51] Three grams of each collected sample was kept in sterilized vials and then were stored at 4°C for further analysis. Pure cultures were obtained by nutrient broth and then were kept in 40% glycerol medium, for long time storage.[52] On the other hand, biosurfactant producing bacteria were screened, based upon preliminary assays. *16SrRNA* sequencing was done for the ID of bacterial isolates.

2.3 | Substrate screening and biosurfactant producers

Parthenium hysterophorusis awed in wild-spread toxic and in vasive species that were collected from Bharathiar University, Coimbatore, Tamil Nadu, and South India. The species were dried under sunlight and powdered to use as a substrate.[49] Bacteria were inoculated and subjected to the production by *P. hysterophorus* as a substrate in an optimized condition at 37°C in 120 rpm for 96 hours and after it were analyzed. Then, the culture floating was gained through centrifugation (15 minutes at 7000 rpm), filtration (0.22-micron filter), acidification (6 N HCl to pH of 2.0) and then allowed for a habitation into 4°C for 12 hours. Glycolipid production was
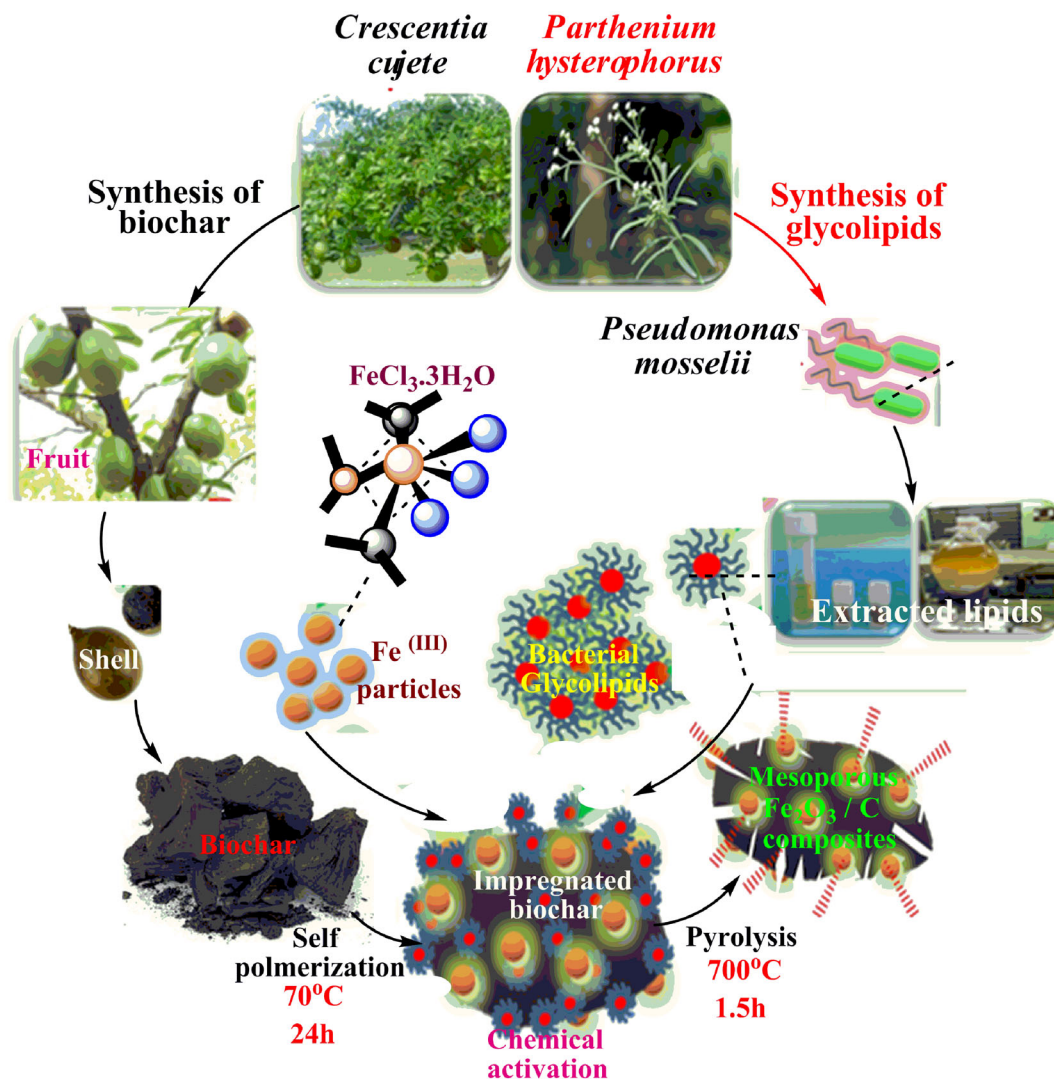
FIGURE 1 Synthesis scheme of RC, GAC and GMAC composites

achieved binate with a mix of methanol: chloroform (2:1. v/v) concentration and then kept for independent shaken, the mixtures were stayed to withstand for a complete phase exchange. The bacterial amphiphilic glycolipid biosurfactants consist of alkyl ether bonds and are linked to sugar moieties (C_5), thereby create both hydrophilic and hydrophobic region. The hydrophilic region effectively enhances the surface interactions via a colloid osmotic mechanism and complexation process with nearby metal ionic species that all result in the formation of areas with improved permeability/pores. Moreover, such an interaction in the form of an active layer will improve the even space between the carbon particles and metal ions, also will create the oxygen rich atmosphere. As a result, under certain pyrolysis process such biosurfactnts form homogenous mesoporous structures.[53] The seized solvent phase was vaporized and the collected jelly-like materials were treated in methanol and

concentrated again by vaporization of the solvent, which yields an almost pure form of glycolipid (Figure S1).[54] The NMR spectra of both the determined and biologically produced glycolipids were depicted in Figure S2.

2.4 | Preparation of Fe_3O_4/porous carbon composites (CCBs)

Crescentia cujete fruit was collected from Bharathiar University, Coimbatore, India. Further separating the *Crescentia cujete* fruit shell (CCFS) sample, it was initially cleaned with double distilled water and dried at direct sunlight for 2 days. The moisture free 50 g dry CCFS powder was pre-pyrolysised at 200°C for 2 hours, to produce raw biochar (Yield: 36%), further it was located in a ball mill (Fritsch Model: Pulverisette 7.0) to obtain their pore size, not more than 0.075 mm. Then 10 g of the

weighed raw biochar was directly mixed with glycolipid: $FeCl_3 \cdot 3H_2O$ precursor in 0.1:1 M ratio. The solution mixer was executed in hot air oven under 70°C for 24 hours. Now, the lipid and iron particles were fully adopted with shell particles thoroughly. The dry mixer was transferred to the silica crucible, under pyrolysis at 700°C for 90 minutes under N_2 gas (30 lbs/min) condition due to the loss of production yield. Immersion of lipid dispersion from the ACs was removed by distilled water. Remaining dispersible impurities were removed continuously by washing with double distilled water until neutral pH (= 7.0). The final product of mesoporous CCBs was consequently desiccated by keeping in oven at 102°C for 6 hours and sieved 60-350 AST net to get a pure precipitate.

2.5 | Material characterization

Glycolipid activated magnetic carbon was synthesized successfully and characterized via XRD by using Xpert pro analytical X-ray Diffractometer Cu Kα radiation (λ = 0.15406 nm). A non-reflective silicon sample holder was used to minimize the background. Nitrogen (N_2). Adsorption/desorption analysis was conducted at a temperature of −196°C, using a Micromeritics ASAP 2020, after degassed at a temperature of 200°C for 5 hours. The morphological and elemental analyses were carried out by SEM with EDX, using Hitachi-SU 8230. The chemical nature of the materials was analyzed by using XPS with Multiprobe photoelectron spectroscopy (Omicron Nanotechnology, Germany) with Al K-alpha source (1486.6 eV) with high-resolution hemisphere analyzer, supported by a neutralizer.

2.6 | Adsorption experiments

Adsorption activities of Fe_2O_3/C composites were applied in the absence of DCF, under laboratory batch experimental conditions. Initially, 10 mg/L of DCF containing water medium was stirred for 12 hours. Then, 50 mL of the stock solution of DCF and 50 mg of adsorbent were added into the 250 mL conical flask, which was adjusted to the acidic pH and alkaline pH using 0.1 M HCl and NaOH solution, respectively. Further, all the adsorption optimization processes were conducted with constant atmospheric heat and an agitation level of 200 rpm for mixing on a digital automated shaker (Bluefic Industrial & Scientific Technologies, India). Before spectrometric analysis, the sample was centrifuged at 5000 rpm to 5 minutes for phase separation. Moreover, the highest solubility of DCF in water is 50 mg/mL.

2.7 | Fabrication of CCBs modified GCE electrode

Initially, the bare GCE was carefully polished several times, using alumina slurries (0.3 and 0.05 μm) on polishing cloth and washed with a 1:1 ratio of ethanol and deionized water to remove physically adsorbed alumina particles and some other impurities. Then, the polished GCE was further treated with 0.1 M H_2SO_4 throughout the potential cycling with −0.2 to 1.0 V at a sweep rate 50 mV/s and thoroughly washed with deionized water. Then GCE was dried under a high purity N_2 stream. Initially, 5 μL GMAC suspensions (1 mg/mL EtOH) dropped cast on the pre-cleaned GCE electrode surface and allowed to dry at environmental temperature. The developed GMAC/GCE electrode was rinsed with electrolyte solution, before electrochemical measurements.

2.8 | Instrumentation for supercapacitance

The electrochemical measurements were carried out, using a standard conventional three-electrode system, using biologic (SB-150) potentiostat. The bare GCE and synthesized GMAC nanocomposite was utilized as a working electrode (surface area 0.071 cm^2), platinum coil and saturated Ag/AgCl electrode were used as references. In addition, the electrochemical impedance spectroscopy was performed in similar equipment with FRA software and all the electrochemical investigation were performed with Na_2SO_4.

3 | RESULTS AND DISCUSSION

3.1 | Materials

The X-ray diffraction patterns of the prepared RC, porous GAC and porous GMAC have shown in Figure 2A. The x-ray diffraction peak positions of the RC and GAC were found to be in the 2θ range at 25° and 45°, which are clearly inconsistent with (002) and (101) reflection planes. The clear observation of the sharp peak of (002) reflection position on the X-ray diffraction pattern for the porous GAC confirms a reasonable crystalline nature, after the activation by using glycolipid to compare the RC. The XRD patterns of the iron oxide incorporated porous GMAC shown in Figure 2A. The resulting reflection patterns of the XRD confirm the formation of α-Fe_2O_3/GAC, labeled as GMAC. The peak positions at 2θ = 24.37, 33.37, 35.86, 41.04, 49.68, 54.30, and
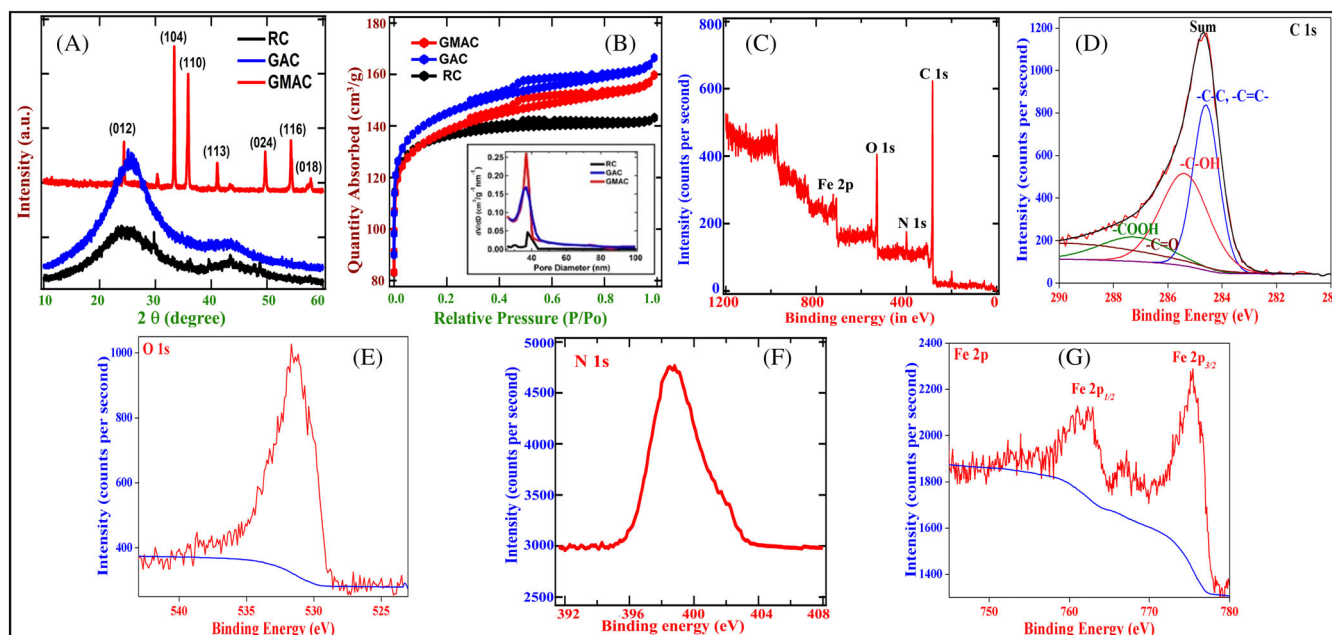
FIGURE 2 A, Powder x–Ray diffraction patterns for the RC (black), GAC (blue), GMAC (red); B, Nitrogen adsorption/desorption isotherms RC (black), GAC (blue), GMAC (red) (Inset: Pore size distributions); C, Survey spectrum of GMAC and high resolution XPS of spectra of, D, C1s, E, O1s, F, Fe2p and, G, N1S

57.80 nm clearly matched with the reflection pattern of (102), (104), (110), (113), (024), (116), and (018), which is consistent with the hexagonal crystalline system of the α-Fe$_2$O$_3$ (JCPDS 86-0550). To determine the specific surface area and porous nature of the prepared RC, the GAC and GMAC materials, the nitrogen adsorption/desorption isotherms measurements were carried out and shown in Figure 2B. From Figure 2B, type-IV isotherms with a hysteresis loop were observed at 0.4 relative pressure regions that confirm a dominant mesoporous structure along with a low-pressure region, observed in the isotherm related to the microporous filling. In addition, the plateau observed in high relative pressure region corresponds to the multilayer adsorption by the mesopores of the prepared materials. The calculated specific surface area of the prepared RC, GAC, and GMAC was found to be 98.83, 456.4, and 466.9 m^2/g, respectively.

XPS measurements were carried out to study the surface elemental composition of the prepared GMAC. The survey spectrum (Figure 2C) confirmed the elemental composition of GMAC with C, O, and Fe, without any other impurities. To study the oxidation states and chemical components present in the C 1s region of the prepared GMAC material, the high-resolution XPS measurement were carried out and it was curve fitted into four different individual peaks: graphitic carbon (284.2-284.5 eV), –C–OH (285.5-285.7 eV), –C=O

(286.8-287 eV), and –COOH (288.9-289.2 eV), which are depicted in Figure 2D,E, respectively. Furthermore, Figure 2F,G shows the survey spectra of other existing inner species viz. Oxygen 1s, N1s, and Iron 2p in the Fe$_2$O$_3$/porous carbon composite structure.

The surface morphology was thoroughly investigated, using FE-SEM and the pictograph is shown in Figure 3. All the surface morphology of the RC, GAC, and GMAC exhibited numerous amounts of meso- and macropores with pore size in the range of 10 to 40 nm, which are originated from the cellulose and hemicelluloses, present in the tropical fruit waste by decomposition and depolymerization process in nitrogen atmosphere. The RC possesses (Figure 3A,B) rock-like surface morphology (average pore size is 40 nm) with lesser pores, when compared to both GAC and GMAC. GAC contains significantly increased amount of pores with an average size of 25 nm (Figure 3C,D), due to the addition of biologically inspired activating agents (glycolipid), which creates larger pores and cavities on the surface of the material. Moreover, incorporation of iron oxide on the material surface, during the activation process significantly increases the number of pores (with average pore size of 10 nm) and cavities (Figure 3E,F). By the closer observation, the incorporation of iron oxide played a crucial role in the formation of pores and cavities with similar pore diameters on the surface of the GMAC material.

FIGURE 3 SEM micrograph of, A and B, RC, C and D, GAC and, E and F, GMAC products were derived from *Crescentia cujete* fruit shell at different magnifications
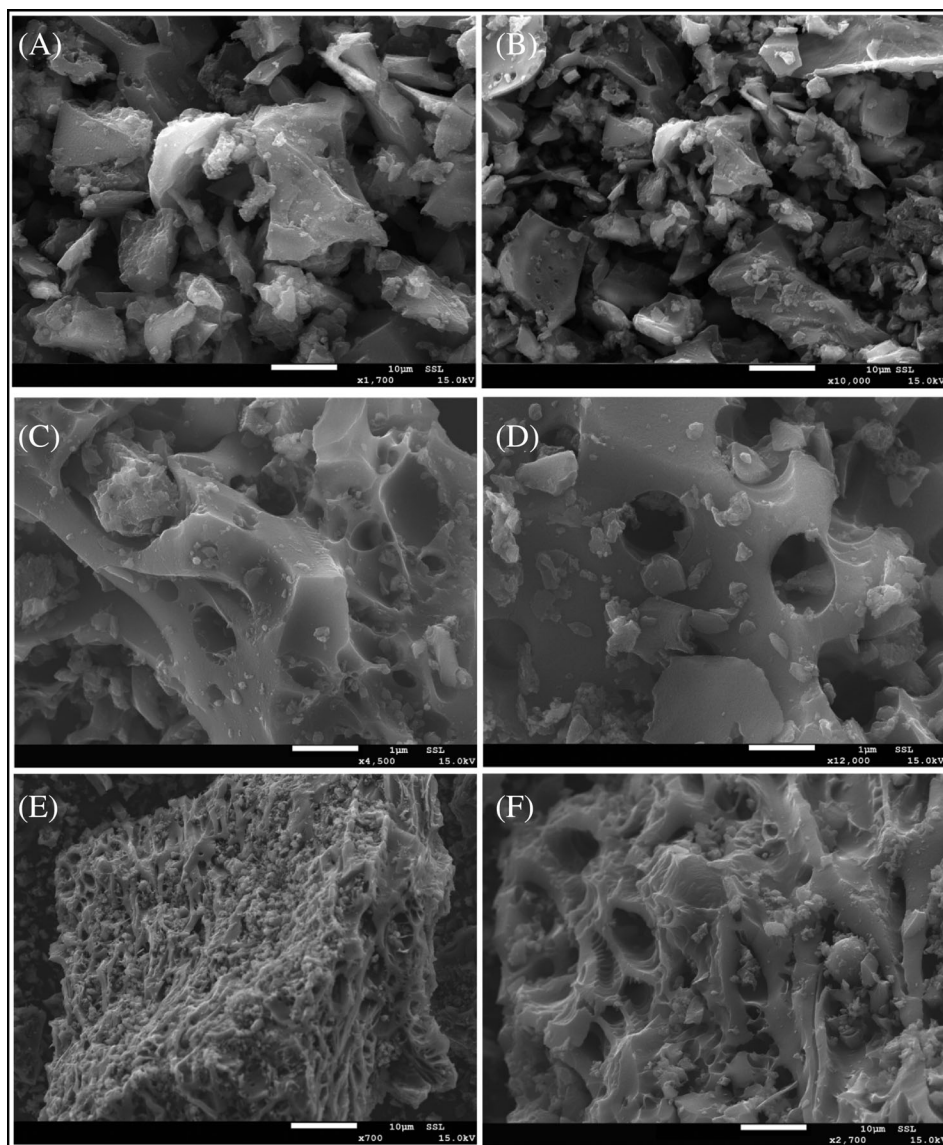
3.2 | DCF treatment studies

3.2.1 | Effect of pH on adsorption

The initial pH of the aqueous medium is the key fact, influencing the adsorption treatment of DCF. The deviation of adsorption possibilities for the adsorbent at various pH ranges probably depend on the chemistry of DCF onto CCBs, particularly the surface-active charge on the adsorbent in solution at a certain pH. Figure 4A shows the pH effect on the adsorption performance of CCBs onto DCF. The pH diagrammatic representation reveals that the absence of pharmaceutical drug pollutant from aqueous medium through the improved GACs decreased with increasing pH, due to the repulsive electrostatic behaviors between the negative surface charge on the CCBs adsorbents and the negatively charged anionic forms of DCF (O^- and COO^-). At this point, the

favorable fixed pH condition is found to be 5, because the DCF cannot fully disperse at pH = 3, also the COO^- functional anionic forms on DCF can certainly act with the positive adsorbent molecules.[33,55]

3.2.2 | Effect of reaction time

The effects of the different adsorption time intervals between 10 and 180 minutes on the adsorption capacity were examined (Figure 4B). The results show that q_e of CCBs increased gradually and rapidly that consequently increased to 60 minutes. Thereby, such a treatment certainly made the system to attain equilibrium after 60 minutes; this was due to increasing treatment time and the possible adsorption spots on the adsorbent that covered later constantly. Thus, the DCF removal rate decreases, after the attainment of certain equilibrium.[56,57]

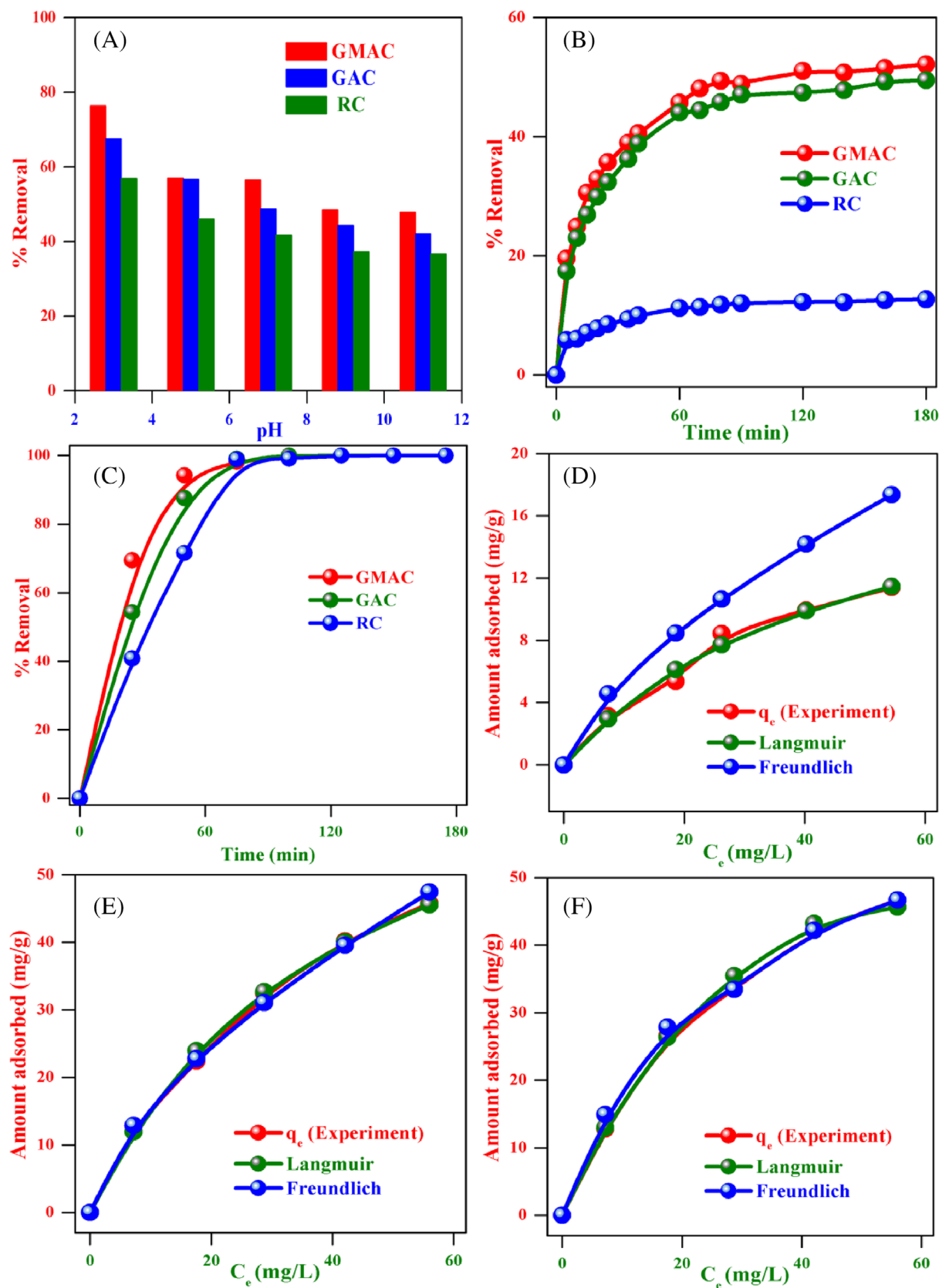**FIGURE 4** DCF Adsorption activities of DCF onto RC, GAC, and GMAC materials: A, Effect of pH on adsorption/desorption process (3-11), B, Effect of treatment time (5-180 minutes), (C) effect of adsorbent dose (25-175 mg) on during adsorption treatment, D, E, and F were the isotherm comparisons of RC, GAC, and GMAC adsorbents, respectively (50 mL of 50 mg/L DCF solution is used for all the adsorption experiments)

Later, all the adsorption parameters were done within 60 minutes of the optimal treatment time for the CCBs.

3.2.3 | Effect of adsorbent mass

The necessity to study the influence of adsorbent mass arises from the economic concern deals with a profitable quantity of adsorbent for effective drug removal. As Figure 4C shown that the DCF removal rate (in %) increased, while increasing CCBs masses, and then for a certain residual doses, it was detected that a limited change in removal efficiency despite the increasing concentration of CCBs. It was obviously found that the increase in the mass of adsorbent enriches the surface site, which becomes increased the number of individual adsorption phases. Thus, also advancement of the chemistry between the CCBs and DCF noted to the increase in the extent of DCF removal onto CCBs.[58] Thereby, the mass of adsorbent indirectly afflicted the adsorption capacity of CCBs. Hence, the CCBs mass increased from 25 to 100 mg/L, the amount of drug removed per unit weight of CCBs decreased, affecting a decrease in adsorption capacity. This finding can be applied to a significant range of adsorption sites at higher adsorption mass for a fixed volume and concentration of DCF.[59]

3.3 | Kinetic studies

The kinetic calculation of DCF treatment by CCBs was investigated to assess the adsorption rate from aqueous medium, which principally depends on the drug adsorption. From Table S1, the pseudo-first and second-order models were linear-fit into the experimental results for the determination of influence rate-controlling steps of the DCF sorption kinetics. It was found that the R^2 significance for the pseudo-second-order model was similar to 1.0 and the calculated DCF adsorption amount at equilibrium (q_e) of 11.4, 45.7, and 45.8 mg/g was also more similar to RC, GAC, and GMAC's experimental results, which were 12.7, 56.2, and 52.6 mg/g. It represents that the DCF adsorption onto CCBs follows the pseudo-second-order kinetics model. Hence, the adsorption treatment was organized via the chemical reactions that involved valence band into conduction band between the adsorbent and adsorbate.[60] According to the discussion, introducing biosurfactants into carbon materials is greatly profitable for DCF removal, based on such functional actions that would improve the affinity for the porous rocks like carbon structure toward DCF however; there exist the electrostatic attractions and dipole-dipole moments.

3.4 | Isotherms

Adsorption isotherm of DCF was investigated by Langmuir and Freundlich models. The non-linear plots of these two isotherm models for RC, GAC and GMAC experimental data were given in Table 1 and Figure 4D-F were the isotherm comparisons of RC, GAC, and GMAC adsorbents. Langmuir isotherm concludes the absence method is monolayer. Each adsorbate or adsorbent poses similar activation energies as well as enthalpies and there is no chemical bond with the adsorbed molecules. Freundlich isotherm concludes that the adsorbent active sites are heterogenic type and hence to the heat of adsorption.[61] In short, Figure 4 clearly shows the comparison plots of two isotherm models for the removal of DCF onto CCBs, and the thorough parameters of Langmuir and Freundlich calculations for the adsorption of DCF, which were indexed in Table S2. In addition, the CCBs experimental data shows that the Langmuir isotherm model exactly describes the adsorption of DCF, which has perfect correlation efficiency (R^2) over the Langmuir model. We can also optimize that the maximum DCF adsorption capacity of RC, GAC, and GMACs obtained were 20.9%, 55.9%, and 77.5%, respectively, which is in magnificent achievement for the adsorption of hydrophobic natured pharmaceutical pollutants.

3.5 | Regeneration and reusability of CCBs

In economical point of view, the regeneration and reusability of the adsorbent is an important factor. Five sequent sorption/desorption cycles were therefore implemented to assess the recovery of GMAC for DCF

TABLE 1 Langmuir and Freundlich isothermal data models of DCF adsorption onto RC, GAC, and GMAC

Isotherms	Variables	RC	GAC	GMAC
Langmuir	Q_e exp. (mg/g)	11.39	45.69	45.79
	q_e cal. (mg/g)	11.47	43.91	45.53
	Q_0 (mg/g)	20.87	55.86	77.51
	R_L	0.308	0.128	0.282
	Δq (%)	9.02	10.95	4.81
	R^2	0.910	0.978	0.983
Freundlich	K_F (L/g)	1.20	8.38	3.707
	n	1.496	2.366	1.579
	Q_e cal (mg/g)	17.36	45.33	47.44
	Δq (%)	51.61	0.69	3.01
	R^2	0.973	0.978	0.996

(100 mg/L). The recovery efficiency of DCF drug was 71.4% in the first cycle, after adsorption for 60 minutes. Further, second and third cycles lead to the desorption rate, still above 65%. The significant reduction rate in desorption efficiency during such a 5 cycles may be attributed to the inadequate desorption of DCF on GMAC.[62] However, this data showed that the as-synthesized CCBs were proficient reusable adsorbents that can be simply reactivated by the treatment of HCl and NaOH solutions (Figure 4A).

3.6 | Cyclic voltammetry measurements of CCBs/GCE modified electrode

The voltammetric behavior of RC, GAC, and GMAC modified electrode was performed by cyclic voltammetry (CV) in 1 M Na_2SO_4 at a scan rate of 50 mV/s and is presented in Figure 5A. All the well developed and modified

electrodes show rectangular shape, indicating a purely capacitive behavior. Interestingly, the GMAC modified electrode shows highest current density and is compared to RC and GAC modified electrodes, due to faradaic current contribution, associated with complex formation with iron species on GAC composite. While the redox peak current responses on iron are not clearly observed on CV, due to the cell configuration limit and the GMAC modified electrode current slightly increases the other total current density that may be related to the first order kinetic effects. Based on these results, the GMAC shows highest current density for other electrodes. Further, we have demonstrated the galvanostatic charge/discharge profile (GCD) of RC, GAC, and GMAC modified electrode at constant current of 2 mA and are given in Figure 5B. The specific capacitance of GMAC can be calculated by the GCD profile curve, according to the equation: $C_s = (I \times \Delta t) / (m \times \Delta V)$, which are 374 F/g (0.2 A/g), 342 F/g (0.4 A/g), 300 F/g (1.0 A/g), 253 F/g (2.0 A/g), 184 F/g (4.0 A/g), and
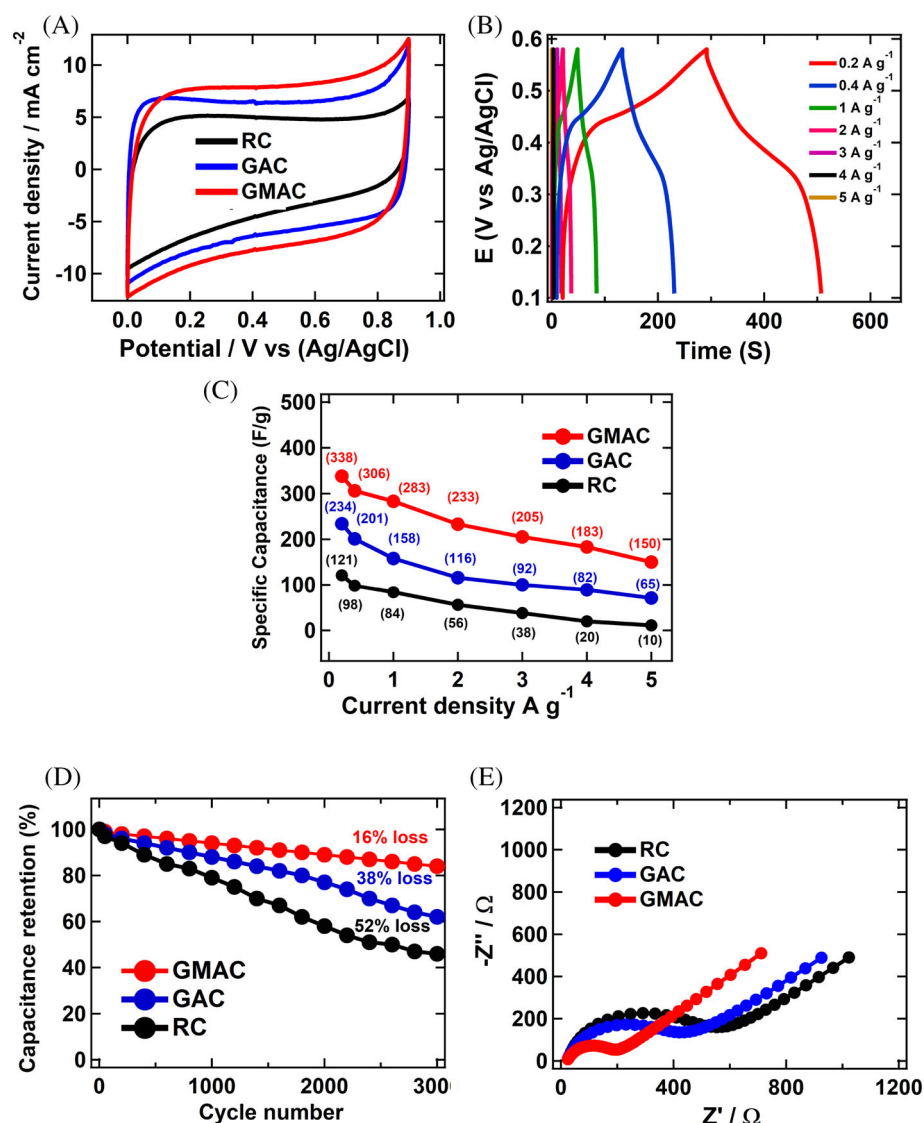

FIGURE 5 A, The CV curves of RC, GAC, and GMAC at a scan rate 50 mV/s, B, galvanostatic charge/discharge curves of GMAC at the current density of 0.2-5.0 Ag^{-1}, C, dependence of the specific capacitance of the RC, GAC, and GMAC on the current density, D, capacitance retention after 3000 cycles, and, E, electrochemical impedance spectra of RC, GAC and GMAC in 0.1 M KCl containing 2.5 mM $[Fe(CN_6)]^{4-/3-}$

TABLE 2 Comparison of various iron composites in electrochemical capacitance performance

S.No	Compound name	Specific capacitance (F/ g)	Electrolyte	References
1	C-Fe/PANI/NI–GF	94.6 (1.0 A/g)	1 M NaNO$_3$	63
2	Fe-doped nano–MnO$_2$	267.0 (0.1 A/g)	1 M Na$_2$SO$_4$	64
3	Fe$_2$O$_4$-carbon nanosheets	163.4 (1.0 A/g)	1 M KOH	65
4	ZnFe$_2$O$_4$	131.0 (1.0 A/g)	1 M KOH	66
5	Fe$_3$O$_4$ nanoparticles	65.4 (1.0 A/g)	6 M KOH	67
6	Fe$_3$O$_4$/rGO	220.1 (1.0 A/g)	6 M KOH	67
7	GMAC	300.0 (1.0 A/g)	1 M Na$_2$SO$_4$	This study

152 F/g (5.0 A/g) that shows an excellent voltammetric performance, due to the formation of highly ordered porous structure on the surface of the GMAC (Figure 5C). Further, the specific capacitance of RC and GAC/GCE is given in Table S3. It also can be seen from the GCD curve that GMAC exhibits good coulombic efficiency and reversibility for its nearly symmetrical charge-discharge profile. The GMAC exhibits excellent voltammetric properties and is due to the complex formation of iron species. In addition, due to the rich natural alkali metal elements in the plant ducts, the self-activation effect can be generated in the carbonization process that significantly increases the specific surface area. Furthermore, we demonstrated the capacitance retention of RC, GAC, and GMAC electrodes that enable us to retain 48%, 62%, and 84%, after 3000 charge-discharge cycles and are presented in Figure 5D. These observations ensure that the GMAC shows excellent stability, when compared to the RC and GAC materials, is due to the complex formation of iron species on GMAC.

Electrochemical impedance spectroscopy (EIS) was used to assess the charge transfer resistance (R_{ct}) of the fabricated electrodes between the electrode/electrolyte solutions. Figure 5E displays the Nyquist curve of RC, GAC, and GMAC modified electrodes in 0.1 M KCl, containing a mixture of potassium ferro and ferric cyanide solution. In order to fit the impedance data using elements such as Warburg impedance (Z_w), constant phase element (CPE), charge-transfer resistance (R_{ct}), and electrolyte solution resistance (R_s). The charge transfer resistance can be measured by the semicircular diameter. It is noticed that RC modified electrode displays a higher R_{ct} of 547 Ω. Further, with the activated raw carbon, the R_{ct} is decreased at 413 Ω. On subsequent modification with GMAC, again R_{ct} is decreased at 171 Ω, which clearly shows that there was a decrease in the resistance associated with ion penetration from the complex iron species deposition. Such a decrease may indicate the facilitation in the penetration of ions due to the resulting porosity. Further, the electrochemical potential outcomes were compared with the previous reports of iron-based electrochemical capacitance materials (Table 2).[68]

4 | CONCLUSIONS

Currently, a structure of glycolipid functionalized-iron-based porous carbon composite materials have largely been used as electrodes with exceptional morphology for high-performance SCs in support of the energy storage devices, owing to their excellent electrochemical behavior, environmental benevolent nature and mechanical flexibility. In this view cheaper, greener and sustainable synthesis of highly porous rock-like carbon from a waste biomass, namely, *Crescentia cujete* fruit shell were carried out and RC, GAC, and GMAC were synthesized, characterized and tested for their adsorption capacity of DCF. A maximum adsorption DCF was achieved onto RA, GAC, and GMAC forecast via Langmuir isotherm model, which were of about 20.87, 55.8, and 77.5 mg/g, respectively. It implies that the adsorption treatment is close-fitting with the *pseudo*-second order model. Based on the environmental remedies and electrochemical storage findings, the biomass can efficiently be represented as bio-surfactant-based surface activation, which is an excellent framework.

DATA AVAILABILITY STATEMENT
The data that support the findings of this study are available from the corresponding author upon reasonable request.

ORCID
Paskalis Sahaya Murphin Kumar https://orcid.org/0000-0002-2688-1825
Ala'a H. Al-Muhtaseb https://orcid.org/0000-0003-0114-077X
Gopalakrishnan Kumar https://orcid.org/0000-0002-7848-5138

REFERENCES

1. Nanaji K, Rao TN, Varadaraju U, Anandan S. Jute sticks derived novel graphitic porous carbon nanosheets as Li-ion battery anode material with superior electrochemical properties. *Int J Energy Res.* 2020;44(3):2289-2297.

2. Sun W, Zhang Y, Yang Z, Yang F. High-performance activated carbons for electrochemical double layer capacitors: effects of morphology and porous structures. *Int J Energy Res.* 2020;44(3): 1930-1950.

3. Zhao J, Zhou C, Li Y, et al. Nickel cobalt oxide nanowires–modified hollow carbon tubular bundles for high–performance sodium–ion hybrid capacitors. *Int J Energy Res.* 2020;44:er5185.

4. Lim S, Pang YL, Shuit SH, Wong KH, Leong CK. Synthesis and characterization of monk fruit seed (Siraitia Grosvenorii)-based heterogeneous acid catalyst for biodiesel production through esterification process. *Int J Energy Res.* 2020;44:er5007.

5. Hong P, Liu X, Zhang X, et al. Hierarchically porous carbon derived from the activation of waste chestnut shells by potassium bicarbonate (KHCO3) for high–performance Supercapacitor electrode. *Int J Energy Res.* 2020;44(2):988-999.

6. Su Y, Liu L, Zhang S, et al. A green route for pyrolysis poly–generation of typical high ash biomass, Rice husk: effects on simultaneous production of carbonic oxide–rich syngas, phenol–abundant bio–oil, high-adsorption porous carbon and amorphous silicon dioxide. *Bioresour Technol.* 2020;295:122243.

7. Wang T, Yang Q, Wang Y, Wang J, Zhang Y, Pan W. Arsenic release and transformation in co–combustion of biomass and coal: effect of mineral elements and volatile matter in biomass. *Bioresour Technol.* 2019;297:122388.

8. Shahid A, Ishfaq M, Ahmad MS, et al. Bioenergy potential of the residual microalgal biomass produced in City wastewater assessed through pyrolysis, kinetics and thermodynamics study to design algal biorefinery. *Bioresour Technol.* 2019;289:121701.

9. Li K, Chen G, Li X, et al. High–temperature dielectric properties and pyrolysis reduction characteristics of different biomass-pyrolusite mixtures in microwave field. *Bioresour Technol.* 2019;294:122217.

10. Lim S, Pang YL, Shuit SH, Wong KH, Leong CK. Synthesis and characterization of monk fruit seed (Siraitia Grosvenorii)–based heterogeneous acid catalyst for biodiesel production through esterification process. *Int J Energy Res.* 2020;44:er5007.

11. Ma G, Yang Q, Sun K, et al. Nitrogen–doped porous carbon derived from biomass waste for high–performance supercapacitor. *Bioresour Technol.* 2015;197:137-142.

12. Tian Y, Lan X, Song Y, Liu C, Zhou J. Preparation and characterization of formed activated carbon from fine blue–coke. *Int J Energy Res.* 2015;39(13):1800-1806.

13. Hadi P, Xu M, Ning C, Sze Ki Lin C, McKay G. A critical review on preparation, characterization and utilization of sludge-derived activated carbons for wastewater treatment. *Chem Eng J.* 2015;260:895-906.

14. Salinas-Torres D, Lozano-Castelló D, Titirici MM, et al. Electrochemical behaviour of activated carbons obtained via hydrothermal carbonization. *J Mater Chem A.* 2015;3(30):15558-15567.

15. Zhu X, Liu Y, Zhou C, Luo G, Zhang S, Chen J. A novel porous carbon derived from hydrothermal carbon for efficient adsorption of tetracycline. *Carbon N Y.* 2014;77:627-636.

16. Farid G, Roy PG, Kruk M. Characterization of micelle-templated silica nanotubes and nanotube bundles using tilt–series transmission electron microscopy. *Microporous Mesoporous Mater.* 2020;293:109760.

17. Parthiban V, Akula S, Sahu AK. Surfactant templated nanoporous carbon–nafion hybrid membranes for direct methanol fuel cells with reduced methanol crossover. *J Membr Sci.* 2017;541:127-136.

18. Kumar HV, Huang KYS, Ward SP, Adamson DH. Altering and investigating the surfactant properties of graphene oxide. *J Colloid Interface Sci.* 2017;493:365-370.

19. Meng Y, Gu D, Zhang F, et al. Ordered Mesoporous polymers and homologous carbon frameworks: amphiphilic surfactant templating and direct transformation. *Angew Chemie – Int Ed.* 2005;44(443):7053-7059.

20. Banham D, Feng F, Burt J, Alsrayheen E, Birss V. Bimodal, templated mesoporous carbons for capacitor applications. *Carbon.* 2010;107:448-473.

21. Rismani E, Fooladi J, Ebrahimi Por GH. Biosurfactant production in batch culture by a bacillus Licheniformis isolated from the Persian Gulf. *Pak J Biol Sci.* 2006;9(13):2498-2502.

22. Vijayakuma S, Saravanan V. Biosurfactants–types, sources and applications. *Res J Microbiol.* 2015;10(5):181-192.

23. Cameotra SS, Makkar RS. Recent applications of biosurfactants as biological and immunological molecules. *Curr Opin Microbiol.* 2004;7(3):262-266.

24. Banat IM, Makkar RS, Cameotra SS. Potential commercial applications of microbial surfactants. *Appl Microbiol Biotechnol.* 2000;53(5):495-508.

25. Cameotra SS, Makkar RS. Synthesis of biosurfactants in extreme conditions. *Appl Microbiol Biotechnol.* 1998;50(5): 520-529.

26. Devaraj S, Sabapathy PC, Nehru L, Preethi K. Bioprocess optimization and production of biosurfactant from an unexplored substrate: *Parthenium hysterophorus. Biodegradation.* 2019;30 (4):325-334.

27. Pradhan AK, Rath A, Pradhan N, Hazra RK, Nayak RR, Kanjilal S. Cyclic lipopeptide biosurfactant from bacillus tequilensis exhibits multifarious activity. *Biotech.* 2018;8(6):261.

28. Priyadarshini E, Pradhan N, Pradhan AK, Pradhan P. Label free and high specific detection of mercury ions based on silver Nano–liposome. *Spectrochim Acta – Part A Mol Biomol Spectrosc.* 2016;163:127-133.

29. Durairaj K, Senthilkumar P, Priya V, Velmurugan P, Jagadeesh Kumar A. Novel synthesis of *Chrysanthemum indicum* flower as an adsorbent for the removal of direct Congo red from aqueous solution. *Desalin Water Treat.* 2018;113:270-280.

30. Egorova KS, Gordeev EG, Ananikov VP. Biological activity of ionic liquids and their application in pharmaceutics and medicine. *Chem Rev.* 2017;117(10):7132-7189.

31. Fick J, Söderström H, Lindberg RH, Phan C, Tysklind M, Larsson DGJ. Contamination of surface, ground, and drinking water from pharmaceutical production. *Environ Toxicol Chem.* 2009;28(12):2522.

32. Ganesan S, Amirthalingam M, Arivalagan P, et al. Absolute removal of ciprofloxacin and its degraded byproducts in aqueous solution using an efficient electrochemical oxidation process coupled with adsorption treatment technique. *J Environ Manag.* 2019;245:409-417.

33. Lonappan L, Rouissi T, Kaur Brar S, Verma M, Surampalli RY. An insight into the adsorption of diclofenac on different

biochars: mechanisms, surface chemistry, and thermodynamics. *Bioresour Technol*. 2018;249:386-394.

34. Larous S, Meniai A-H. Adsorption of Diclofenac from aqueous solution using activated carbon prepared from olive stones. *Int J Hydrogen Energy*. 2016;41(24):10380-10390.

35. De Luna MDG, Budianta W, Rivera KKP, Arazo RO. Removal of sodium Diclofenac from aqueous solution by adsorbents derived from cocoa pod husks. *J. Environ. Chem Eng*. 2017;5(2):1465-1474.

36. Coimbra RN, Calisto V, Ferreira CIA, Esteves VI, Otero M. Removal of pharmaceuticals from municipal wastewater by adsorption onto pyrolyzed pulp mill sludge. *Arab J Chem*. 2019;12(8):3611-3620.

37. Antunes M, Esteves VI, Guégan R, Crespo JS, Fernandes AN, Giovanela M. Removal of Diclofenac sodium from aqueous solution by Isabel grape bagasse. *Chem Eng J*. 2012;192:114-121.

38. Qu WH, Xu YY, Lu AH, Zhang XQ, Li WC. Converting biowaste corncob residue into high value added porous carbon for supercapacitor electrodes. *Bioresour Technol*. 2015;189:285-291.

39. Bi Z, Kong Q, Cao Y, et al. Biomass-derived porous carbon materials with different dimensions for supercapacitor electrodes: a review. *J Mater Chem A*. 2019;7(27):16028-16045.

40. Han J, Wang H, Yue Y, et al. A self–healable and highly flexible supercapacitor integrated by dynamically cross–linked electro-conductive hydrogels based on nanocellulose-templated carbon nanotubes embedded in a viscoelastic polymer network. *Carbon*. 2019;149:1-18.

41. Liu T, Zhang L, Cheng B, Yu J. Hollow carbon spheres and their hybrid nanomaterials in electrochemical energy storage. *Adv Energy Mater*. 2019;9:1803900.

42. Liu H, Zhang S, Chen Y, et al. Rational design of TiO_2@nitrogen-doped carbon coaxial nanotubes as anode for advanced lithium ion batteries. *Appl Surf Sci*. 2018;458:1018-1025.

43. Hu D, Chen C, Liu Q. Fabrication of hollow carbon spheres with robust and significantly enhanced capacitance behaviors. *J Mater Sci*. 2018;53(27):12310-12321.

44. Chen A, Wang Y, Yu Y, et al. Nitrogen-doped hollow carbon spheres for supercapacitors. *J Mater Sci*. 2017;52:3153-3161.

45. Chen Z, Ye S, Evans SD, et al. Confined assembly of hollow carbon spheres in carbonaceous nanotube: a spheres-in-tube carbon nanostructure with hierarchical porosity for high-performance supercapacitor. *Small*. 2018;14:1704015.

46. Zhang L, Shi D, Huang TJ, Huang R, Gong H. Light enhanced energy storage ability through a hybrid plasmonic Ag nanowire decorated hydroxide "skin structure". *Nanoscale*. 2017;9:18430-18437.

47. Shen K, Ran F, Zhang X, et al. Supercapacitor electrodes based on nano-polyaniline deposited on hollow carbon spheres derived from cross-linked co-polymers. *Synth Met*. 2015;209:369-376.

48. Molina-Sabio M, Rodriguez-Reinoso F. Role of chemical activation in the development of carbon porosity. *Colloids Surf A Physicochem Eng Asp*. 2004;241(1):15-25.

49. Devaraj S, Sabapathy PC, Nehru L, Preethi K. Bioprocess optimization and production of biosurfactant from an unexplored substrate: *Parthenium hysterophorus*. *Biodegradation*. 2019;30(4):325-334.

50. Sabarinathan D, Chandrika SP, Venkatraman P, Easwaran M, Sureka CS, Preethi K. Production of polyhydroxybutyrate (PHB) from pseudomonas Plecoglossicida and its application towards cancer detection. *Informatics Med Unlocked*. 2018;11:61-67.

51. Devaraj S, Amirthalingam M, Sabapathy PC, Govindan S, Palanisamy S, Kathirvel P. Anthelmintic efficacy of glycolipid biosurfactant produced by pseudomonas Plecoglossicida: an insight from mutant and transgenic forms of *Caenorhabditis elegans*. *Biodegradation*. 2019;30(4):203-214.

52. Ismail H, Ijah U, Riskuwa M, Allamin I. Biodegradation of spent engine oil by bacteria isolated from the Rhizosphere of legumes grown in contaminated soil. *Int J Environ*. 2014;3(2):63-75.

53. Kaustuvmani P, Rupshikha P, Mohan CK, Suresh D. Characterization of biosurfactant produced during degradation of hydrocarbons using crude oil as sole source of carbon. *Front Microbiol*. 2017;8:279.

54. Parthipan P, Sabarinathan D, Angaiah S, Rajasekar A. Glycolipid biosurfactant as an eco–friendly microbial inhibitor for the corrosion of carbon steel in vulnerable corrosive bacterial strains. *J Mol Liq*. 2018;261:473-479.

55. Liang XX, Omer AM, Hu Z, Wang Y, Yu D, Ouyang X. Efficient adsorption of diclofenac sodium from aqueous solutions using magnetic amine-functionalized chitosan. *Chemosphere*. 2019;217:270-278.

56. Luo H, Zhang Y, Xie Y, et al. Iron-rich microorganism–enabled synthesis of magnetic biocarbon for efficient adsorption of diclofenac from aqueous solution. *Bioresour Technol*. 2019;282:310-317.

57. Bhadra BN, Seo PW, Jhung SH. Adsorption of diclofenac sodium from water using oxidized activated carbon. *Chem Eng J*. 2016;301:27-34.

58. Ahmad R. Studies on adsorption of crystal violet dye from aqueous solution onto coniferous Pinus bark powder (CPBP). *J Hazard Mater*. 2009;171(1–3):767-773.

59. Bhattacharyya KG, Sharma A. *Azadirachta indica* leaf powder as an effective biosorbent for dyes: a case study with aqueous Congo red solutions. *J Environ Manag*. 2004;71(3):217-229.

60. Sotelo JL, Ovejero G, Rodríguez A, Álvarez S, Galán J, García J. Competitive adsorption studies of caffeine and diclofenac aqueous solutions by activated carbon. *Chem Eng J*. 2014;240:443-453.

61. Ghaedi M, Nasab AG, Khodadoust S, Rajabi M, Azizian S. Application of activated carbon as adsorbents for efficient removal of methylene blue: kinetics and equilibrium study. *J Ind Eng Chem*. 2014;20(4):2317-2324.

62. Kalagatur NK, Karthick K, Allen JA, et al. Application of activated carbon derived from seed shells of *Jatropha curcas* for decontamination of Zearalenone mycotoxin. *Front Pharmacol*. 2017;8:760.

63. Khamlich S, Abdullaeva Z, Kennedy JV, Maaza M. High performance symmetric supercapacitor based on zinc hydroxychloride nanosheets and 3D graphene–nickel foam composite. *Appl Surf Sci*. 2017;405:329-336.

64. Wang Z, Wang F, Li Y, Hu J, Lu Y, Xu M. Interlinked multiphase Fe–doped MnO_2 nanostructures: a novel design for enhanced pseudocapacitive performance. *Nanoscale*. 2016;8(33):7309-7317.

65. Liu D, Wang X, Wang X, et al. Ultrathin nanoporous Fe_3O_4-carbon nanosheets with enhanced supercapacitor performance. *J Mater Chem A*. 2013;1(6):1952.

66. Zhu M, Zhang X, Zhou Y, Zhuo C, Huang J, Li S. Facile solvothermal synthesis of porous $ZnFe_2O_4$ microspheres for capacitive pseudocapacitors. *RSC Adv*. 2015;4(49):39270-39277.

67. Qi T, Jiang J, Chen H, Wan H, Miao L, Zhang L. Synergistic effect of Fe_3O_4/reduced graphene oxide nanocomposites for supercapacitors with good cycling life. *Electrochim Acta*. 2013;114:674-680.

68. Krishna Prasad G, Rajesh Babu D. Shape engineered three dimensional α-Fe_2O_3-activated carbon nano composite as enhanced electrochemical supercapacitor electrode material. *Int J Energy Res*. 2018;42(15):4687-4696.

SUPPORTING INFORMATION

Additional supporting information may be found online in the Supporting Information section at the end of this article.